Population of the yrast superdeformed band in ^{152}Dy within a cluster approach

A. S. Zubov,[1] V. V. Sargsyan,[1,2] G. G. Adamian,[1] and N. V. Antonenko[1]
[1]*Joint Institute for Nuclear Research, 141980 Dubna, Russia*
[2]*Yerevan State University, 0025 Yerevan, Armenia*
(Received 28 May 2013; revised manuscript received 24 August 2013; published 20 September 2013)

By using the dinuclear system approach combined with quantum diffusion and statistical methods, the population of the yrast superdeformed band in the ^{152}Dy nucleus is treated. The excitation functions are calculated and analyzed for the population of the superdeformed states in xn, pxn, and αxn evaporation channels of different asymmetric and almost symmetric reactions. The dependencies of the relative intensities of $E2$ transitions between the rotational states of the superdeformed band on the de-excitation channels, charge asymmetry of the entrance channel, and beam energy are established. The restrictions of the population of the superdeformed band in spin by complete fusion and quasifission processes are shown. The calculated results are compared with the available experimental data.

DOI: 10.1103/PhysRevC.88.034607 PACS number(s): 25.70.Jj, 24.10.−i, 24.60.−k

I. INTRODUCTION

Superdeformed (SD) nuclear states were initially discovered in actinides at low spins [1]. Subsequently, the effect of superdeformation has been observed at high spins in different regions of the nuclear chart [2]. The SD states of nuclei with mass numbers $A \sim 150$ are still of theoretical and experimental interest. The SD states of several isotopes of Dy, Gd, and Tb [2] have been produced in different evaporation channels of fusion-evaporation reactions with population intensities of about 1%. The measured moments of inertia are about $80\hbar^2$/MeV, which correspond to the quadrupole deformation parameters $\beta_2 \sim 0.6$. For these states, one can observe the rotational γ transitions from very high ($\sim 60\hbar$) to lower ($\sim 20\hbar$) spins and, in some cases, determine the energy of the lowest observed state of the SD band. The experimental achievements have stimulated the theoretical description of the SD states and the mechanism of their population. The observed nuclear properties of SD states are similar in different nuclei with $A \sim 150$ [2]. Therefore, in this paper we focus only on the population of the SD band in ^{152}Dy, first discovered and experimentally studied in the best way [3–14].

Investigations of the high-spin SD rotational bands in different mass regions have been performed with the cranked Woods-Saxon and Nilsson models [15,16] using a few deformation parameters and with the cluster models where the cluster degrees of freedom, taken properly, allow us to simplify the treatment of a nuclear system in the space of collective coordinates. The coexistence of the clustering and of mean-field aspects is a unique feature of nuclear many-body systems [17,18]. There have been many recent developments in the field of nuclear clusters including the ability to perform *ab initio* calculations of the light nuclei, such as Green's function Monte Carlo methods [19] and antisymmetrized molecular or fermionic dynamics approaches [20,21]. Semimicroscopic symmetry-adopted cluster approaches have been applied to predict the SD and hyperdeformed (HD) states in light nuclei [17,18,22,23]. The calculations for light nuclei have shown that the configurations with large quadrupole and octupole deformation parameters and the low-lying collective negative-parity states are strongly related to clustering [16,22–30]. As known from the study of light nuclei, the SD shape of nuclei can be considered as dinuclear rather than ellipsoidal. The experimental and theoretical results provide us with evidence for the existence of fission modes by the clustering of fissioning nuclei [31]. Strong collective dipole transitions between the excited SD band and the lowest-energy SD band in ^{150}Gd, ^{152}Dy, ^{190,194}Hg, and $^{196–198}$Pb and between the yrast SD band and the ND band in ^{194}Hg and ^{194}Pb have been observed [5,32]. This indicates the possibility that the transitions are affected by the existence of a pronounced cluster structure of SD states.

Based on the theoretical results of Refs. [33–42], one can be convinced that certain quasimolecular configurations with dumbbell shapes have the same quadrupole moments and moments of inertia as those measured for high- and low-spin SD states and low-spin HD isomer states. With the dinuclear system (DNS) approach [34,37,39–42], the main properties of SD states in the ^{60}Zn nucleus and several isotopes of Pb and Hg have been described. In this model, two clusters are in a touching configuration and the main collective coordinate is the charge (mass) asymmetry. The relative distance between the centers of the clusters corresponds to the minimum of the nucleus-nucleus interaction potential and is slightly larger than the sum of cluster radii. The overlapping of nuclei is hindered by a repulsive nucleus-nucleus interaction potential at smaller relative distances. In the cluster models [36,38], the charge (mass) asymmetry coordinate is fixed, and the main collective coordinate is the relative distance between the centers of the clusters. Because of this, the clusters penetrate each other.

According to the DNS approach [34,37,39–42], the strongly deformed nuclear state can be treated as the cold rotating DNS (in which the internal excitation energy is zero). At given angular momentum the potential pocket of the nucleus-nucleus potential contains the quasibound states with quite large half-lives. The lowest quasibound state seems to be identical to the SD (HD) state in the case of asymmetric (more symmetric)

DNS configuration. As shown within the cluster and statistical approaches, the highly deformed states can be populated in the capture process [without the compound nucleus (CN) formation stage] either by de-excitation (neutron emission) of the initial DNS formed in the entrance channel at collision energy above the Coulomb barrier [43] or directly by tunneling through this barrier [40,44]. Using the same approach, in the present paper we will consider the population of the SD states in the reactions with different entrance-channel asymmetries. However, the SD cluster states of interest will be located quite far from the entrance-channel configuration and reached by nucleon transfer. Note that in the literature there are only rather schematic calculations of the population of the SD band and the relative intensities of $E2$ transitions between the rotational states of the SD band [45].

II. MODEL

A. Population of the SD state in fusion-evaporation reactions

According to the DNS approach [34,37,39–42], the SD state can be considered as the cold rotating DNS. Its formation can be treated as a two-step process. First, the colliding nuclei pass over the Coulomb barrier and form the initial excited DNS (two nuclei in a touching configuration) in the entrance channel. After the capture, the DNS is trapped in the pocket of the interaction potential between partners or in the local minimum of the potential energy surface. Second, this initial DNS evolves by diffusion in the charge Z and mass A asymmetry coordinates (where Z and A are the charge and mass numbers of the DNS light nucleus) and transforms into the SD state related to the DNS which is quite different from the initial one. This transformation is accompanied by de-excitation due to particle emission and the DNS decay in the coordinate of the relative distance R between the centers of nuclei. The proposed mechanism for populating the SD state is schematically presented in Fig. 1. Here, U is the potential energy of the DNS (see the next section). The cold DNS corresponding to the SD state is formed by evolution of the initial DNS toward a more asymmetric DNS configuration. The DNS configuration is trapped in the potential minimum both in Z, A and in R coordinates and lives rather a long time to be interpreted as the SD state. Such a system can possibly emit γ quanta between collective rotational states and these can be can be experimentally observed.

The partial cross section

$$\sigma_{\rm SD}(E_{\rm c.m.}, L) = \sigma_{\rm cap}(E_{\rm c.m.}, J) P_{\rm SD}(E_{\rm c.m.}, J) \qquad (1)$$

of the population of the SD state with spin L depends on the capture cross section $\sigma_{\rm cap}$, which is related to the formation of the excited initial DNS, and the probability $P_{\rm SD}$ of transformation of this DNS into the SD state (cold rotating DNS). Here, $E_{\rm c.m.}$ is the bombarding energy in the center-of-mass system, $J = L + \Delta L$ is the initial angular momentum, and ΔL is the average angular momentum carried by the evaporated particles.

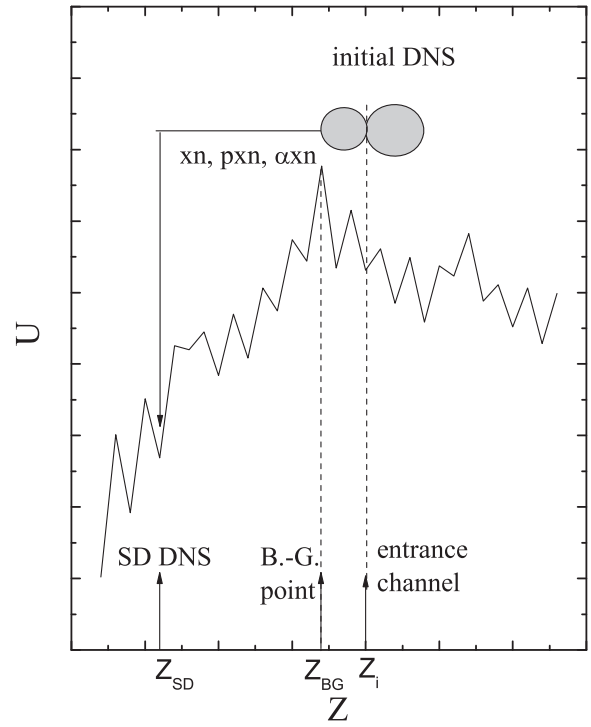

FIG. 1. Scheme of the formation of the SD state in an asymmetric reaction. Z is the charge number of the DNS light nucleus. Z_i and $Z_{\rm SD}$ are the charge asymmetries of the initial entrance-channel DNS and SD DNS, respectively. The Businaro-Gallone point $Z_{\rm BG}$ is marked.

B. DNS potential energy and the nucleus-nucleus interaction potential

Under the assumption of a small overlap of the nuclei in the DNS its potential energy is calculated as follows [46]:

$$U(R, Z, A, J) = B_1 + B_2 + V(R, Z, A, \beta_1, \beta_2, J) - \left[B_{12} + E_{12}^{\rm rot}(J)\right], \qquad (2)$$

where B_1 and B_2 are the mass excesses of the fragments in their ground states, and β_1 and β_2 are their quadrupole deformation parameters, which are taken from Ref. [47] for even-even nuclei. For the quadrupole deformation parameter of an odd nucleus, we choose the maximal value from the deformation parameters of neighboring even-even nuclei. The experimental values of B_1 and B_2 in Ref. [48] are used if available. Otherwise, we use the values from Ref. [49]. The potential energy is normalized to the potential energy $B_{12} + E_{12}^{\rm rot}(J)$ of the rotating CN [the sum of the mass excess B_{12} and rotational energy $E_{12}^{\rm rot}(J)$]. The nucleus-nucleus potential

$$V(R, Z, A, \beta_1, \beta_2, J) = V_C(R, Z, \beta_1, \beta_2) + V_N(R, A, \beta_1, \beta_2) + V_{\rm rot}(A, \beta_1, \beta_2, J) \qquad (3)$$

in (2) is the sum of the Coulomb potential V_C, the nuclear potential V_N, and the centrifugal potential $V_{\rm rot} = \hbar^2 J(J+1)/(2\Im)$. Because the overlap of nuclei in the DNS is quite small, the DNS moment of inertia $\Im$ is calculated in the sticking limit as

$$\Im = k_0(\Im_1 + \Im_2 + \mu R^2). \qquad (4)$$

For large angular momenta L, the moments of inertia $\Im_i$ ($i = 1, 2$) of the DNS nuclei are obtained in the rigid-body approximation as

$$\Im_i = \frac{1}{5} m_0 A_i \left(a_i^2 + b_i^2\right),$$
$$a_i = R_{0i}\left(1 - \frac{\beta_i^2}{4\pi}\right)\left(1 + \sqrt{\frac{5}{4\pi}}\beta_i\right), \quad (5)$$
$$b_i = R_{0i}\left(1 - \frac{\beta_i^2}{4\pi}\right)\left(1 - \sqrt{\frac{5}{16\pi}}\beta_i\right).$$

As known from the experimental study, the moments of inertia of strongly deformed nuclear states are very close to 85% of those in the rigid-body limit [33]. In our calculations we set $k_0 = 0.85$ for the DNS with $Z < Z_{\rm BG}$ and $k_0 = 1$ for the DNS with $Z \geqslant Z_{\rm BG}$. Here, $Z_{\rm BG}$ is the value of charge asymmetry in the Bussinaro-Gallone point (the position of the maximum of U; see Fig. 1). In the entrance channel (the capture stage) $\Im = \mu R^2$, where μ is the reduced mass of relative motion.

For the nuclear part, we use the double-folding formalism with the Skyrme-type effective density-dependent nucleon-nucleon interaction [37,46,50]. The densities of the nuclei are taken in the Woods-Saxon form with the nuclear radius parameter $r_0 = 1.02$–1.16 fm and the diffuseness parameter $a = 0.48$–0.56 fm, depending on the charge and mass numbers of the nucleus [37]. Due to the sum of the repulsive Coulomb and centrifugal summands with the attractive nuclear one in Eq. (3), the nucleus-nucleus potential has a potential pocket with a minimum situated for pole-pole orientation at the distance $R = R_m \approx R_1[1 + \sqrt{5/(4\pi)}\beta_1] + R_2[1 + \sqrt{5/(4\pi)}\beta_2] + 0.5$ fm (where $R_i = r_0 A_i^{1/3}$ fm). The position of the Coulomb barrier corresponds to $R = R_b \approx R_m + 1$ fm in the DNS considered. The quasifission barrier B_R^{qf}, calculated as the difference between the bottom of the potential pocket and the top of the Coulomb barrier (Fig. 2), prevents the decay of the DNS in the R degree of freedom. The barriers $B_Z^{\rm sym}$ and $B_Z^{\rm asym}$ hinder the drift and diffusion of the SD DNS toward more symmetric and more asymmetric configurations in Z, respectively.

The nucleus-nucleus potential V as a function of R and the potential energy U at $R = R_m(\eta)$ as a function of Z are presented in Fig. 2 at different angular momenta J. For each Z, we minimized $U(R_m, Z, A, J)$ with respect to A. The values of barriers B_R^{qf} and $B_Z^{\rm asym,sym}$ for the DNS corresponding to the SD state are also shown. While the depth B_R^{qf} of the potential pocket decreases with increasing angular momentum J and is equal to zero at the critical angular momentum $J = J_{\rm cr}$ due to the large repulsive centrifugal part of the nucleus-nucleus potential (3), the values of $B_Z^{\rm asym,sym}$ vary only slightly with J. Because $B_Z^{\rm asym} < B_Z^{\rm sym}$ in the case considered, the complete fusion (or, in other words, the transition to a normally deformed state) from a given cluster configuration is more probable than the diffusion in the charge (mass) asymmetry coordinate to smaller asymmetry. The potential energy of more symmetric DNS configurations decreases faster with angular momentum, in comparison with asymmetric ones, since the moments of inertia of these DNS are larger and, thus, the positive contributions from the centrifugal term in Eq. (3) to U are smaller. One can also introduce the value of angular momentum J_0 at which the potential energy of the almost symmetric DNS configuration becomes smaller than that of the CN configuration. For ^{152}Dy, we obtain $J_0 \approx 60$. At $J_{\rm cr} > J > J_0$ the cold DNS can be trapped in the minimum of potential energy at the symmetric DNS configuration, the complete fusion becomes energetically denied, and the DNS decay (quasifission) becomes the dominant process.

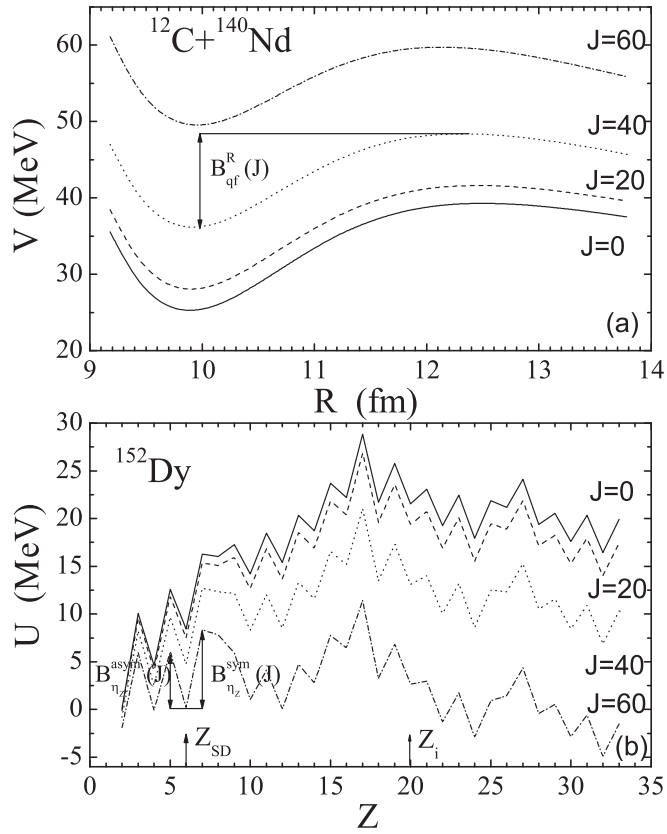

FIG. 2. (a) Dependencies of the nucleus-nucleus potential V on R for a cluster configuration which corresponds to the SD state of ^{152}Dy. The definition of B_R^{qf} is illustrated. (b) The DNS potential energy as a function of charge number Z of the DNS light nucleus for ^{152}Dy. The value of U is normalized to the energy of the rotating CN ^{152}Dy. The calculated results at $J = 0$, 20, 40, and 60 are presented by solid, dashed, dotted, and dashed-dotted curves, respectively. The definitions of $B_\eta^{\rm sym}$ and $B_\eta^{\rm asym}$ are illustrated.

C. Capture cross section

The partial capture cross section $\sigma_{\rm cap}(E_{\rm c.m.}, J)$ depends on the capture probability $P_{\rm cap}$, which is related to the transition through the entrance Coulomb barrier (Fig. 2):

$$\sigma_{\rm cap}(E_{\rm c.m.}, J) = \frac{\pi\hbar^2}{2\mu E_{\rm c.m.}}(2J+1)P_{\rm cap}(E_{\rm c.m.}, J). \quad (6)$$

The maximal angular momentum in (6) is $J_{\rm max} = J_{\rm cr}$ at which the pocket in the nucleus-nucleus potential in the entrance channel disappears and the capture does not occur. For the reactions considered, $J_{\rm cr} = 76$–82. The capture probability

$P_{\rm cap}$ is calculated by employing the quantum diffusion approach [51,53,54] (see Appendix A).

D. Transformation of initial excited DNS into a SD cluster state

1. Evolution of the DNS in charge and mass asymmetry coordinates

After the capture stage there are nucleon drift and nucleon diffusion between the nuclei of the DNS. The system evolves either toward the CN configuration or to a more symmetric DNS configuration. Then, a statistical equilibrium is reached in the charge and mass asymmetry coordinates so that the formation probability [55]

$$P_{Z,A} \sim \exp[-U(R_m, Z, A, J)/T_{\max}(J)] \tag{7}$$

of each DNS ($Z \geqslant 2$) or CN ($Z = 0$ and 1) configuration at certain J depends on the potential energy $U(R_m, Z, A, J)$. The CN is taken into consideration with $U(R_m, Z, A, J) = 0$. The temperature in Eq. (7) is taken in the deepest minimum of U:

$$T_{\max}(J) = \max[T_{\rm CN}(J), \{T_{Z,A}(J)\}_{Z\geqslant 2, A\geqslant 2}],$$

where $T_{\rm CN}(J) = [E^*_{\rm CN}(J)/a]^{1/2}$ and $T_{Z,A}(J) = [E^*_{Z,A}(J)/a]^{1/2}$ are the temperatures of the CN with excitation energy $E^*_{\rm CN}(J) = E_{\rm c.m.} + Q - E^{\rm rot}_{12}(J)$ and the DNS with asymmetries (Z, A) and excitation energy $E^*_{Z,A}(J) = E^*_{\rm CN}(J) - U(R_m, Z, A, J)$, respectively. The notation $\{T_{Z,A}(J)\}_{Z\geqslant 2, A\geqslant 2}$ means the set of temperatures of all possible DNS. Here, the Fermi-gas model is employed to calculate the temperatures with a level-density parameter $a = A_t/12$, where A_t is the total mass number of the system.

2. Competition between particle emission and DNS decay

Any excited DNS with $Z \geqslant 2$ existing with probability $P_{Z,A}$ can decay in the R coordinate into two fragments with a probability rate [55]

$$\Lambda^R_{Z,A} \sim \exp\left[-B^{qf}_R(Z, A, J)/T_{Z,A}(J)\right] \tag{8}$$

if the local excitation energy of the DNS is high enough to overcome the barrier $B^{qf}_R(Z, A, J)$ of the nucleus-nucleus potential (Fig. 2). For $0 \leqslant Z < 2$, $\Lambda^R_{Z,A} = 0$. The competition between particle (for example, neutron or proton) emission and the DNS transition over the quasifission barrier B^{qf}_R in R should be considered for all possible DNS and CN configurations. The probability rate for neutron (n) or proton (p) emission from the DNS with $Z \geqslant 2$ is

$$\Lambda^{n,p}_{Z,A} \sim \exp[-B_{n,p}(Z, A)/T_{Z,A}(J)] + \exp[-B_{n,p}(Z_t - Z, A_t - A)/T_{Z,A}(J)], \tag{9}$$

where the emission of particles from both light (first term) and heavy (second term) DNS nuclei is taken into account with the corresponding binding energies $B_{n,p}$ (plus the value of the Coulomb barrier for the proton). Here, Z_t is the total charge number of the DNS. For the emission of a neutron or proton from the CN ($Z = 0$ or 1), the probability rate is defined as

$$\Lambda^n_{Z=0,A=1} \sim \exp[-B_n(Z = 0, A = 1)/T_{\rm CN}(J)] \tag{10}$$

or

$$\Lambda^p_{Z=1,A=1} \sim \exp[-B_p(Z = 1, A = 1)/T_{\rm CN}(J)], \tag{11}$$

where $B_n(Z = 0, A = 1)$ or $B_p(Z = 1, A = 1)$ is the neutron or proton binding energy in the CN. Here, $\Lambda^n_{Z=1,A=1} = \Lambda^p_{Z=0,A=1} = 0$. Analogously, we calculate the probability rates of the deuteron ($Z = 1, A = 2$) and triton ($Z = 1, A = 3$) emissions from the CN [55].

The neutron or proton emission probability $W^{n,p}_{Z,A}(E^*_{\rm CN}, J)$ from the DNS with (Z, A) or the CN is calculated as the product of the DNS or CN formation probability and the particle emission probability rate from this configuration:

$$W^{n,p}_{Z,A} = \frac{P_{Z,A}\Lambda^{n,p}_{Z,A}}{\sum_{Z',A'} P_{Z',A'}\left[\Lambda^R_{Z',A'} + \Lambda^n_{Z',A'} + \Lambda^p_{Z',A'}\right]}, \tag{12}$$

where the indexes Z' and A' run over all possible decay channels from the neutron and proton evaporations to the symmetric splitting. Note that the same statistical approach was applied in Ref. [55] to analyze the light particle and fragment emission from the excited DNS and compound nuclei. The calculated mass and isotopic distributions, as well, as average total kinetic energies of the reactions products, were found to be in a good agreement with the experimental data [55].

3. De-excitation by neutron emission

In the evaporation channel of the emission of x neutrons, the probability of transformation of the initial excited DNS with (Z_i, A_i) into the SD state [cold DNS with $(Z_{\rm SD}, A_{\rm SD})$],

$$P_{\rm SD}(E_{\rm c.m.}, L) = w_{xn}(E_{\rm c.m.}, J)\prod_{k=1}^{x} P^k_n, \tag{13}$$

depends on the probabilities P^k_n of neutron emission from all possible DNS nuclei and CN in the evaporation step k and the probability w_{xn} of realization of the xn-evaporation channel at given J and excitation energy corresponding to the values of $E_{\rm c.m.}$ (see Appendix B). The average angular momentum and energy carried by the neutron are taken as $l_n = 0.5$ and $B_n + 2T(J)$ [where $T(J)$ is the temperature of the DNS or CN configuration], respectively. At the evaporation steps $k = 1, \ldots, (x - 1)$ and last step $k = x$,

$$P^{k<x}_n = \left(\sum_{Z',A'} W^n_{Z',A'}\right)_k \tag{14}$$

and

$$P^{k=x}_n = \left(W^n_{Z_{\rm SD},A_{\rm SD}+1}\right)_{k=x}, \tag{15}$$

respectively. So, at each evaporation step the competition between neutron emission and different binary fragmentations of the excited system (decays of the excited DNSs) is considered. At the last evaporation step [see Eq. (15)], the neutron is emitted from the DNS with $Z = Z_{\rm SD}$ and $A = A_{\rm SD} + 1$.

4. De-excitation by proton and α-particle emission

In the case of proton emission, one can use the same expressions as presented above for calculating $P_{\rm SD}$. The neutron binding energy should be replaced in Eqs. (13), (B1), and (B2) by the sum of the proton binding energy and the Coulomb energy. The average angular momentum carried by protons is taken as $l_p = 0.5$. The evaporation of charge particles likely occurs in the first steps. To calculate w_{pxn} and $w_{\alpha xn}$, one can use the expressions in Appendix B, taking into consideration the Coulomb interaction in the emission thresholds.

In the DNS approach, the emission of an α particle is interpreted as quasifission of the excited DNS being in an α-cluster configuration. An α particle is assumed to be emitted at the first evaporation step. The probability of this process is calculated as

$$W^{\alpha}_{2,4} = P^{k}_{\alpha} = \frac{P_{Z=2,A=4}\Lambda^{R}_{Z=2,A=4}}{\sum_{Z',A'} P_{Z',A'}\left[\Lambda^{R}_{Z',A'} + \Lambda^{n}_{Z',A'} + \Lambda^{p}_{Z',A'}\right]}. \quad (16)$$

The threshold of α-particle emission from the DNS is calculated as

$$B^{qf}_{R}(Z=2, A=4, J) = B^{qf}_{R}(Z=2, A=4, J=0) + \frac{\hbar^2 l_\alpha(l_\alpha+1)}{2k_0\mu}\left(\frac{1}{R_b^2} - \frac{1}{R_m^2}\right). \quad (17)$$

Here, $l_\alpha = \frac{\mu R_m^2}{\Im_1+\Im_2+\mu R_m^2} J$ is the orbital angular momentum carried by the α particle. After the emission of an α particle the average excitation energy of the system decreases by the value $B^{qf}_{R}(Z=2, A=4, J) + 2T_{Z=2,A=4}$ (see Appendix C).

E. Intensity of $E2$ transitions between rotational states of the SD band

The cold rotating SD DNS, being in the potential minimum in (R, Z, A) coordinates, can emit γ quanta because of the transitions between the collective rotational states. The time $T_\gamma(L)$ of the collective $E2$ transition between the rotational SD states with angular momenta L and $L-2$ is written as [47]

$$T_\gamma(L) = \frac{408.1}{5/(16\pi)\left(Q_2^{(c)}\right)^2[E_\gamma(L\to L-2)]^5}, \quad (18)$$

where the energy

$$E_\gamma(L\to L-2) = L(L+1)/(2\Im) - (L-2)(L-1)/(2\Im)$$

of the γ quantum is in units of keV, the electric quadrupole moment

$$Q_2^{(c)} = 2e\frac{A_2^2 Z_1 + A_1^2 Z_2}{A^2}R^2 + Q_2^{(c)}(1) + Q_2^{(c)}(2)$$

of the SD DNS is in $10^2\, e\,\mathrm{fm}^2$, and T_γ is in seconds. The electric quadrupole moments $Q^{(c)}_{\lambda_2}(i)$ $(i = 1, 2)$ of the SD DNS nuclei are calculated in their centers of mass.

The γ transition between the collective rotational SD states competes with the SD DNS decays by tunneling in R (quasifission) and Z coordinates. The tunneling probability in A at fixed $Z = Z_{\rm SD}$ is neglected. The tunneling times through the barrier in R and Z coordinates, respectively, are estimated by using a parabolic approximation for the potential energy surface as ($i = R, Z$, $j =$ qf, asym) [43]

$$T_i = \frac{2\pi}{\Omega_i^j}\left\{1 + \exp\left[2\pi B_i^j \big/ \left(\hbar\omega_i^j\right)\right]\right\}, \quad (19)$$

where Ω_i^j and ω_i^j are the corresponding frequencies in the minimum of the potential energy and on the barrier, respectively, and B_i^j are the heights of barriers for the cold DNS. $B_Z^{\rm asym}$ ($B_Z^{\rm sym}$) is the minimal value of the barrier which prevents the evolution of the DNS in Z to the direction of more asymmetric (symmetric) configurations. For the reactions considered, $B_Z^{\rm asym} < B_Z^{\rm sym}$, and the tunneling in Z to the direction of symmetry (through the barrier $B_Z^{\rm sym}$) can be neglected. The tunneling in Z to the direction of asymmetry leads to the complete fusion of the DNS nuclei.

Using the rates $\Lambda_{\gamma,R,Z} = \hbar/T_{\gamma,R,Z}$ of different competing processes (collective γ transition in the SD band and tunneling in R and Z from the SD minimum on the potential energy surface), one can estimate the probability of the emission of a rotational γ quantum from the SD state with angular momentum L as

$$P_\gamma(L) = \frac{\Lambda_\gamma(L)}{\Lambda_\gamma(L) + \Lambda_R(L) + \Lambda_Z(L)}. \quad (20)$$

The cross section for the $E2$ transition between the rotational states L and $(L-2)$ of the SD band is calculated as

$$\sigma_{\gamma_{\rm SD}}(E_{\rm c.m.}, L) = \sum_{L'=L}^{L_{\max}} \sigma_{\rm SD}(E_{\rm c.m.}, L') \prod_{L''=L}^{L'} P_\gamma(L''), \quad (21)$$

and the relative intensity of this transition is proportional to this cross section:

$$I_{\rm SD}(E_{\rm c.m.}, L\to L-2) = \frac{\sigma_{\gamma_{\rm SD}}(E_{\rm c.m.}, L)}{\sigma^{\max}_{\gamma_{\rm SD}}}, \quad (22)$$

where $\sigma^{\max}_{\gamma_{\rm SD}} = \sigma_{\gamma_{\rm SD}}(E_{\rm c.m.}, L = L^{\max}_{\rm SD}) = \max[\sigma_{\gamma_{\rm SD}}(E_{\rm c.m.}, L), L = 0, \ldots, L_{\max}]$ and $L_{\max} = J_{\max} - \Delta L$.

Using the same approach, one can calculate the γ-transition intensities of the normal deformed (ND) bands in nuclei produced in the fusion-evaporation reactions. Then one can calculate the ratio of SD and ND bands intensities as

$$\frac{I_{\rm SD}}{I_{\rm ND}} = \frac{I_{\rm SD}\left(E_{\rm c.m.}, L^{\max}_{\rm SD}\to L^{\max}_{\rm SD}-2\right)}{I_{\rm ND}\left(E_{\rm c.m.}, L^{\max}_{\rm ND}\to L^{\max}_{\rm ND}-2\right)} = \frac{\sigma_{\gamma_{\rm SD}}\left(E_{\rm c.m.}, L = L^{\max}_{\rm SD}\right)}{\sigma_{\gamma_{\rm ND}}\left(E_{\rm c.m.}, L = L^{\max}_{\rm ND}\right)} = \frac{\sigma^{\max}_{\gamma_{\rm SD}}}{\sigma^{\max}_{\gamma_{\rm ND}}}. \quad (23)$$

Note that $\sigma_{\rm ND}$ is related to $P_{\rm ND}$, which is defined by an expression similar to Eq. (13).

III. CALCULATED RESULTS

A. Cluster SD states of ^{152}Dy

One can choose the DNS configuration that corresponds to the experimentally observed SD state by comparison of the calculated nuclear characteristics of different DNS configurations with the measured ones for the SD state.

Here, we treat the SD states of the ^{152}Dy nucleus with measured moment of inertia $\Im_{SD}^{exp} = (85 \pm 2)\hbar^2/\text{MeV}$ [3], charge quadrupole moment $Q_2^{exp} = (18 \pm 3) \times 10^2\ e\,\text{fm}^2$ [4], and energy $E_{SD}^{exp}(24^+) = 10.64$ MeV [5] of the lowest measured state $L^\pi = 24^+$ of the SD band as the states of the DNS ^{12}C + ^{140}Nd, for which our calculations give the values $\Im_{SD}^{th} = 76\hbar^2/\text{MeV}$, $Q_2^{th} = 11 \times 10^2\ e\,\text{fm}^2$, and $E_{SD}^{th}(24^+) = 9.94$ MeV. As seen in Fig. 2, this DNS is in one the deepest local minima of the driving potential. The depth of the minimum is almost insensitive to the value of J. Another deep local potential minimum corresponds to the DNS ^{8}Be + ^{144}Sm, which has smaller moment of inertia and quadrupole moment and probably contributes to other rotational bands. The minima for more symmetric DNSs are shallower. Because the value of B_R^{qf} decreases with increasing Z, more symmetric DNSs have smaller lifetimes to produce long rotational bands.

B. Population of cluster SD states of ^{152}Dy in the 4n-evaporation channel

1. Capture process

The dependence of the capture cross section on angular momentum is shown in Fig. 3 for the ^{48}Ca + ^{108}Pd reaction at beam energies $E_{lab} = 191$, 197, 205, and 212 MeV. At small angular momenta, the partial capture cross section $\sigma_{cap}(E_{c.m.}, J)$ grow due to the factor $2J + 1$ in Eq. (6), while the decrease of the capture probability P_{cap} due to the increase of the centrifugal term in the nucleus-nucleus potential is rather weak. At larger J, the system of colliding nuclei turns out in the sub-barrier region and the capture cross section drops, since in this region the decrease of P_{cap} with increasing J is not compensated by the factor $2J + 1$. The larger the value of $E_{c.m.}$, the larger value of the angular momentum at which the transition to the sub-barrier regime occurs.

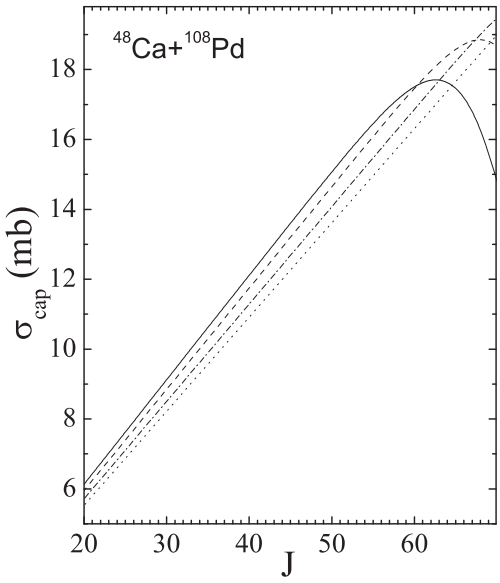

FIG. 3. The calculated partial capture cross sections in the ^{48}Ca + ^{108}Pd reaction at beam energies $E_{lab} = 191$ MeV (solid line), 197 MeV (dashed line), 205 MeV (dash-dotted line), and 212 MeV (dotted line).

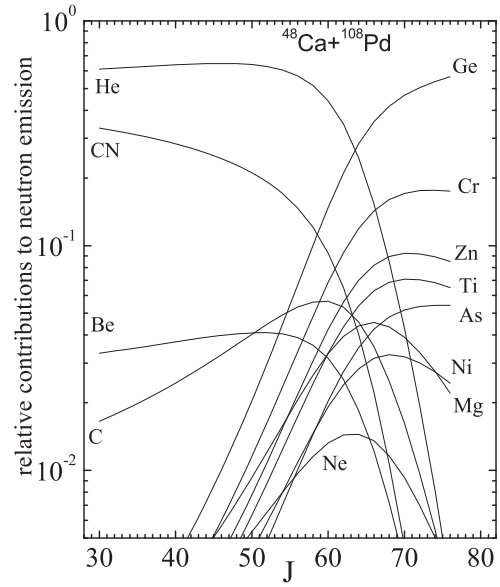

FIG. 4. The calculated relative contributions of the CN and different DNS configurations to the neutron emission as a function of the angular momentum in the ^{48}Ca + ^{108}Pd reaction at beam energies $E_{lab} = 191$ MeV (a) and 205 MeV (b). The lighter nuclei of the DNS are indicated.

2. Transition from an excited initial DNS to a cold SD DNS

At angular momenta $J \leqslant 50$–60, the main contribution to the neutron emission is provided by the excited CN and α-cluster configuration (DNS with the light nucleus ^{4}He), as one can conclude from Fig. 4. In the cluster approach, the wave function of the ND state contains the α-cluster component whose weight increases with J [56]. For higher angular momenta ($J > J_0 \approx 60$), the contributions to neutron emission from symmetric and asymmetric DNS configurations become sufficient. The potential energies of these configurations are comparable to or smaller than those for the CN and α configuration at high angular momenta (see Fig. 2), and their statistical weights become larger.

The potential energy of the DNS ^{12}C + ^{140}Nd ascribed to the SD state increases slower with J than those of the α-cluster configuration and CN. Therefore, the statistical weight of this configuration increases with J, which leads to the increase of factors $P_n^{k=4}$ and $\prod_{k=1}^{4} P_n^k$ (Fig. 5). The moderate growth of the factor $\prod_{k=1}^{4} P_n^k$ at $L \leqslant 50$ is caused by the angular momentum dependence of the probability $P_n^{k=4}$ of neutron emission at the last (fourth) evaporation step [see Eq. (15)]. For higher angular momenta, the statistical weights of almost symmetric DNS configurations are the largest ones, and their quasifission probabilities are larger than the probabilities of neutron emission due to the small values of B_R^{qf} caused by the repulsive Coulomb and centrifugal forces. This leads to the rapid decrease of $\prod_{k=1}^{4} P_n^k$ with increasing J at $J \geqslant 50$.

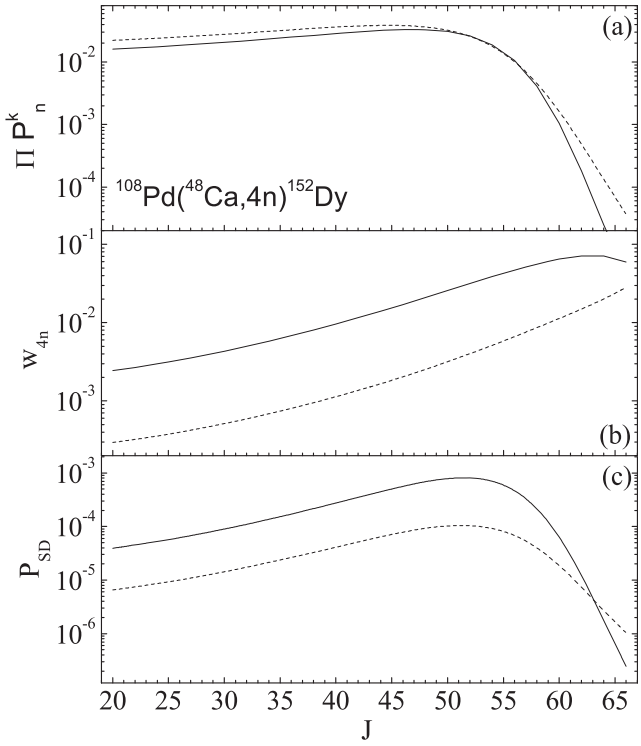

FIG. 5. The calculated dependencies of the factors $\prod_{k=1}^{4} P_n^k$ (a), w_{4n} (b), and $P_{\rm SD}$ (c) on angular momentum J in the ^{48}Ca + ^{108}Pd reaction at beam energies $E_{\rm lab} = 191$ MeV (solid line) and 205 MeV (dashed line).

The influence of the beam energy on the factor $\prod_{k=1}^{4} P_n^k$ is realized through the temperatures $T_{\rm max}(J)$, $T_{Z,A}(J)$, and $T_{\rm CN}(J)$ in Eqs. (7)–(11). At smaller angular momenta the neutron emission from asymmetric DNS configurations prevails over quasifission. Therefore, as follows from Eqs. (7)–(12), the larger values of $E_{\rm lab}$ lead to the larger factors of $\prod_{k=1}^{4} P_n^k$ over this range of J. At larger values of J, the quasifission from almost symmetric DNS configurations is the dominant process, and the opposite effect is observed (Fig. 5). One can also see in this figure that the influence of the beam energy on the factor $\prod_{k=1}^{4} P_n^k$ is rather weak.

The dependence of the factor w_{4n} on J has a Maxwellian-like form with a maximum at the excitation energy at which the realization of the $4n$-evaporation channel is the most probable in comparison with other xn channels. The larger value of $E_{\rm lab}$ leads to a shift of the maximum of the function $w_{4n}(J)$ to larger angular momenta. The growth of w_{4n} and the decrease of $\prod_{k=1}^{4} P_n^k$ at $45 \leqslant L \leqslant 60$ mainly provide the appearance of the maximum in the partial probability $P_{\rm SD}$ (Fig. 5) and, correspondingly, in the cross section $\sigma_{\rm SD}(E_{\rm c.m.}, L)$ at $L = L_{\rm SD}^{\rm opt} \approx 50$ (Fig. 6).

3. SD band intensities

Calculated probabilities of the emission of rotational γ quanta from the SD states of ^{152}Dy are shown in Fig. 7. The angular momentum dependencies of Λ_{R,η_Z} are determined by the angular momentum dependence of the corresponding barriers. While the barrier in Z is weakly affected by the

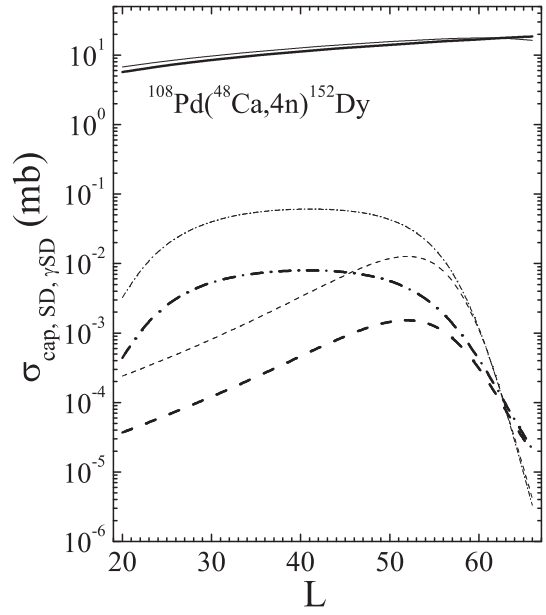

FIG. 6. The calculated dependencies of the cross sections $\sigma_{\rm cap}(E_{\rm c.m.}, J = L + 2)$ (solid lines), $\sigma_{\rm SD}(E_{\rm c.m.}, L)$ (dashed lines), and $\sigma_{\gamma_{\rm SD}}(E_{\rm c.m.}, L)$ (dash-dotted lines) on the spin L in the ^{108}Pd(^{48}Ca,4n) reaction at the beam energies $E_{\rm lab} = 191$ MeV (thin lines) and 205 MeV (thick lines).

change of L, the value of the quasifission barrier, B_R^{qf}, decreases much stronger with increasing L. Therefore, the tunneling in R (quasifission) suppresses the γ emission at large L. At very small angular momentum the $E2$ transition time becomes enormous due to the small values of $E_\gamma(L \to L - 2)$. The dominant process in this range of L is tunneling in Z to a more asymmetric configuration and complete fusion.

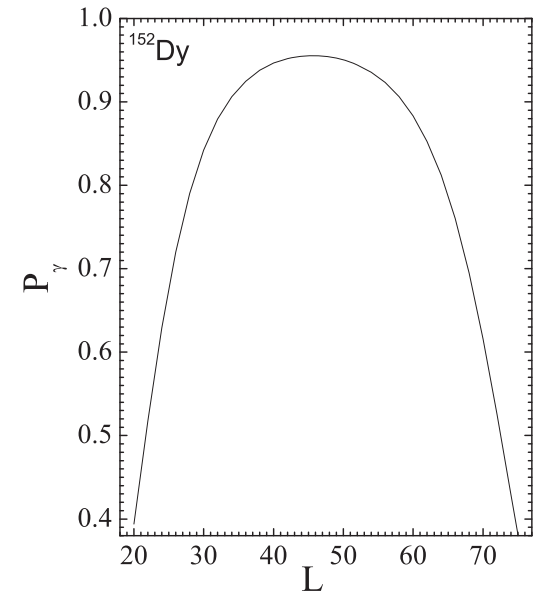

FIG. 7. The calculated probability P_γ of the emission of a rotational γ quantum from the SD state of ^{152}Dy as a function of spin L.

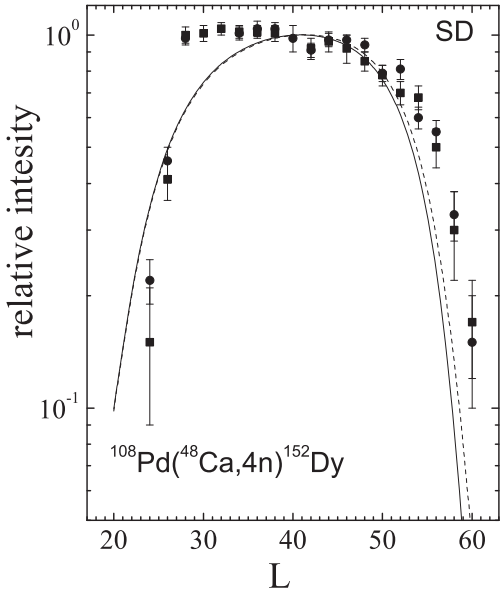

FIG. 8. The measured (symbols) [2,3] and calculated (lines) collective rotational $E2$-transition intensities in the SD band of the ^{152}Dy nucleus produced in the ^{108}Pd(^{48}Ca, $4n$) reaction at beam energies $E_{\rm lab} = 191$ MeV (squares and solid line) and $E_{\rm lab} = 205$ MeV (circles and dashed line).

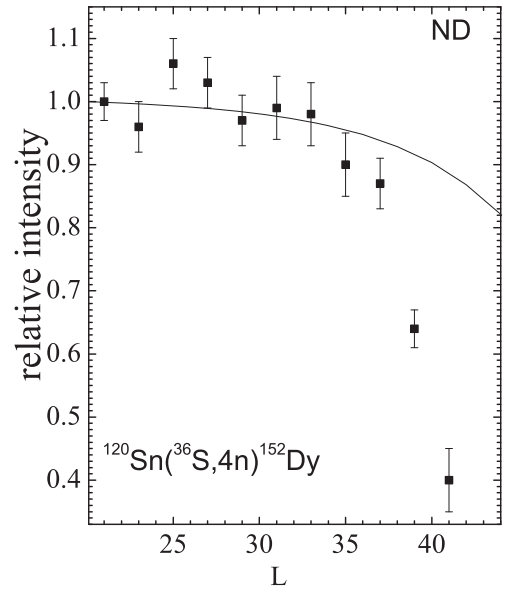

FIG. 9. The measured [7] (squares) and calculated (line) intensities in the ND band in the ^{152}Dy nucleus produced in the ^{120}Sn(^{36}S, $4n$) reaction at beam energy $E_{\rm lab} = 168$ MeV.

The populated SD states with spins near the maximum of $\sigma_{\rm SD}$ (or $P_{\rm SD}$) at $L_{\rm SD}^{\rm opt} \approx 50$ (Figs. 5 and 6) give the main contribution to the cross sections $\sigma_{\gamma_{\rm SD}}(E_{\rm c.m.}, L)$ of the $E2$ transition between the rotational states and play the role of doorway states for a rotational cascade (Fig. 6). At $30 \leqslant L \leqslant 50$ the probabilities P_γ of the emission of rotational γ quanta are close to 1 (see Fig. 7). Therefore, γ emission is the dominant process among the different ways of the populated SD state evolving at these spins. This results in the appearance of a plateau in the function $\sigma_{\gamma_{\rm SD}}(L)$ near its maximum at $L_{\rm SD}^{\rm max} \approx 40$. The fall of the cross section $\sigma_{\gamma_{\rm SD}}$ at large $L \geqslant 50$ is explained by the significant decrease of the quasifission barriers in this region due to the increase of centrifugal forces, which lead to a decrease of $\sigma_{\rm SD}$ and P_γ (see Fig. 6 and 7). At $L \leqslant 25$ the $E2$ transitions in the SD band are suppressed, as their times are too large, and the transition to the ND rotational bands (CN and α configuration) becomes more favorable. The values of $P_{\rm SD}$, $\sigma_{\rm SD}(E_{\rm c.m.}, L)$, and $\sigma_{\gamma_{\rm SD}}$ are rather sensitive to beam energy due to the strong dependence of the factor w_{4n} on $E_{\rm lab}$, as one can see in Figs. 5 and 6. However, the shape of the function $\sigma_{\gamma_{\rm SD}}(L)$ remains almost stable with the variation of beam energy.

In Fig. 8, the measured [2,3,6] and calculated relative transition intensities in the yrast SD rotational band of the ^{152}Dy nucleus produced in the reaction ^{108}Pd(^{48}Ca, $4n$) at bombarding energies $E_{\rm lab} = 191$ and 205 MeV are presented. Our calculated results well represent the dependence of intensities on angular momentum. Note that the very weak dependence of transition intensities on the beam energy found in our calculations is confirmed in the experiment.

The measured [7] and calculated intensities of γ-ray transitions of the alternative parity ND band in ^{152}Dy produced in the reaction ^{120}Sn(^{36}S, $4n$) at $E_{\rm lab} = 168$ MeV are presented in Fig. 9. In the cluster approach, the wave functions of the states of the alternative parity ND band contain an α-cluster component [56]. Since we consider the population of the yrast ND band only in the evaporation process and the transitions to this band from other ND bands are not taken into consideration, there is disagreement with the experimental data at $L > 35$. However, the calculated values are close to the measured ones near the maximum of relative intensity. So, we can estimate the ratio of the SD and ND band intensities with Eq. (23). This ratio is presented in Fig. 10 as a function of beam energy for the ^{108}Pd(^{48}Ca, $4n$) reaction. One can seen a good agreement of the calculated results with the experimental data.

4. Entrance-channel effects

In order to study whether entrance-channel effects influence the production of the SD states and the SD band intensity, we consider the population of the yrast SD band in ^{152}Dy via nearly mass symmetric [^{74}Ge + ^{82}Se (Fig. 11)] and mass asymmetric [^{36}S + ^{120}Sn (Fig. 12) and ^{48}Ca + ^{108}Pd (Fig. 6)] reactions leading to the same CN at similar excitation energies. At energies corresponding to the maximal ratios of the SD and ND band intensities, $\sigma_{\gamma_{\rm SD}}^{\rm max}(^{74}{\rm Ge} + ^{82}{\rm Se}) < \sigma_{\gamma_{\rm SD}}^{\rm max}(^{36}{\rm S} + ^{120}{\rm Sn}) < \sigma_{\gamma_{\rm SD}}^{\rm max}(^{48}{\rm Ca} + ^{108}{\rm Pd})$, because $\sigma_{\rm SD}(^{74}{\rm Ge} + ^{82}{\rm Se}) < \sigma_{\rm SD}(^{36}{\rm S} + ^{120}{\rm Sn}) < \sigma_{\rm SD}(^{48}{\rm Ca} + ^{108}{\rm Pd})$ or $\sigma_{\rm cap}(^{74}{\rm Ge} + ^{82}{\rm Se}) < \sigma_{\rm cap}(^{36}{\rm S} + ^{120}{\rm Sn}) < \sigma_{\rm cap}(^{48}{\rm Ca} + ^{108}{\rm Pd})$. The measured [9,10] and calculated ratios of SD and ND band intensities are presented in Figs. 13 and 14 for the reactions ^{82}Se(^{74}Ge, $4n$) and ^{120}Sn(^{36}S, $4n$), respectively. The calculated values are in a good agreement with the experiment for the asymmetric reaction ^{36}S + ^{120}Sn, but they about half those of the experimental data for the almost symmetric reaction ^{74}Ge + ^{82}Se. No evidence for entrance-channel effects is found in our model, which contradicts with the experimental

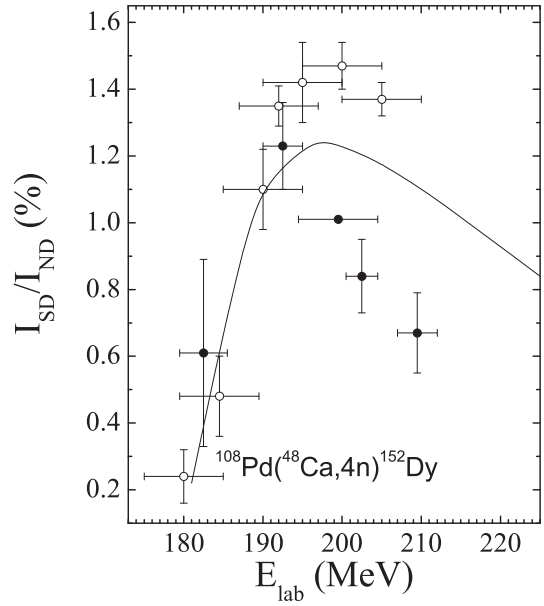

FIG. 10. The calculated ratio of the SD and ND band intensities (line) in the ^{152}Dy nucleus as a function of the beam energy in the ^{108}Pd(^{48}Ca, $4n$) reaction. The experimental data are from Refs. [8] (closed circles) and [10] (open circles).

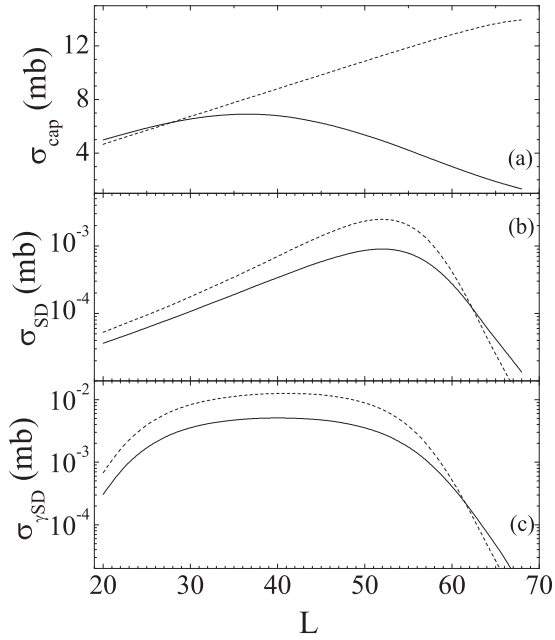

FIG. 11. The calculated dependencies of the cross sections $\sigma_{cap}(E_{\rm c.m.}, J = L + \Delta L)$ (a), $\sigma_{\rm SD}(E_{\rm c.m.}, L)$ (b), and $\sigma_{\gamma_{\rm SD}}(E_{\rm c.m.}, L)$ (c) on the spin L in the reactions ^{80}Ge(^{74}Se, $2n$) (solid line) and ^{82}Se(^{74}Ge, $4n$) (dashed line) at the optimal bombarding energies corresponding to the maximal ratios of the SD and ND band intensities in these reactions.

data results from Refs. [9,10], in which some enhancement of the SD band intensities was observed with respect to the ND band intensities in the case of a symmetric entrance-channel reaction. The largest deviation of the calculated value of $\frac{I_{\rm SD}}{I_{\rm ND}}$ in the ^{74}Ge + ^{82}Se reaction from one in the ^{36}S + ^{120}Sn reaction is found to be about of 5% in the case of the owest considered excitation energy $E^*_{\rm CN}(J = 0) = 62$ MeV, at which $\frac{I_{\rm SD}}{I_{\rm ND}} \approx 0.2$ (Fig. 10). With increasing $E^*_{\rm CN}(J = 0)$ this deviation rapidly decreases. In the experiment [9,10] the difference between two reactions is up to 100%, although the error bars are quite large.

If one fixes the same excitation energy for two different reactions 1 and 2, then the ratio of intensities of the SD and ND bands can be expressed as $[\frac{I_{\rm SD}}{I_{\rm ND}}]_1/[\frac{I_{\rm SD}}{I_{\rm ND}}]_2 = [\frac{\sigma^{\rm max}_{\gamma_{\rm SD}}}{\sigma^{\rm max}_{\gamma_{\rm ND}}}]_1/[\frac{\sigma^{\rm max}_{\gamma_{\rm SD}}}{\sigma^{\rm max}_{\gamma_{\rm ND}}}]_2 \approx [\frac{\sigma^{\rm max}_{\rm SD}(E_{\rm c.m.}, L^{\rm opt}_{\rm SD})}{\sigma^{\rm max}_{\rm ND}(E_{\rm c.m.}, L^{\rm opt}_{\rm ND})}]_1/[\frac{\sigma^{\rm max}_{\rm SD}(E_{\rm c.m.}, L^{\rm opt}_{\rm SD})}{\sigma^{\rm max}_{\rm ND}(E_{\rm c.m.}, L^{\rm opt}_{\rm ND})}]_2 \approx [\frac{P_{\rm cap}(E_{\rm c.m.}, L^{\rm opt}_{\rm SD})}{P_{\rm cap}(E_{\rm c.m.}, L^{\rm opt}_{\rm ND})}]_1/[\frac{P_{\rm cap}(E_{\rm c.m.}, L^{\rm opt}_{\rm SD})}{P_{\rm cap}(E_{\rm c.m.}, L^{\rm opt}_{\rm ND})}]_2$. For the reactions considered, the spins $[L^{\rm opt}_{\rm SD,ND}]_1 \approx [L^{\rm opt}_{\rm SD,ND}]_2$, and these values vary in the interval from 50 to 56. The capture probabilities for the reactions ^{120}Sn(^{36}S, $4n$), ^{108}Pd(^{48}Ca, $4n$), and ^{82}Se(^{74}Ge, $4n$) calculated at the same excitation energy $E^*_{\rm CN}(J = 0) = 62$ MeV are presented in Fig. 15. One can see that the bombarding energy is higher than the entrance barrier at optimal angular momentum for all reactions considered and the values of capture probabilities $P_{\rm cap}(E_{\rm c.m.}, J)$ are slightly less than 1 in the angular momentum interval of interest. So, the capture probabilities are close to each other and there is no entrance-channel effect in the calculated ratio of the SD and ND band intensities. Hence, the entrance-channel effect requires additional experimental and theoretical studies.

C. Evaporation-channel effects

The population and properties of the SD states of ^{152}Dy have been also experimentally studied in different de-excitation channels of the reactions ^{80}Se(^{74}Ge, $2n$) [11], ^{124}Sn(^{33}S, $5n$) [12], ^{120}Sn(^{37}Cl, $p4n$) [13], and ^{123}Sb(^{37}Cl, $\alpha 4n$) [14]. To analyze the dependence of the SD band intensity on the de-excitation channel and beam energy, we calculate the excitation functions for the population of the SD band in ^{152}Dy produced in these reactions. Dependencies of the cross sections $\sigma_{\rm cap}(E_{\rm c.m.}, J)$, $\sigma_{\rm SD}(E_{\rm c.m.}, L)$, and $\sigma_{\gamma_{\rm SD}}(E_{\rm c.m.}, L)$ on J and L for these reactions are presented in Figs. 11, 12, and 16. The calculations are performed at beam energies corresponding to the maximal ratios of the SD and ND band intensities (Figs. 13, 14, and 17).

As follows from Figs. 6, 11, 12, and 16, the excitation functions for the population of the SD band are similar to ones for the CN reactions, but they are much broader. The widths of the calculated excitation functions increase with number of evaporated particles. This is similar to the CN reactions as well. The values of $\sigma_{\rm SD}$ and $\sigma^{\rm max}_{\gamma_{\rm SD}}$ for the $4n$ de-excitation channel is close to those for the $5n$ channel, as the decrease of $\prod_{k=1}^{5} P_n^k$ in comparison with $\prod_{k=1}^{4} P_n^k$ is compensated by larger $\sigma_{\rm cap}$ in the ^{33}S + ^{124}Sn reaction than in the ^{36}S + ^{120}Sn reaction (Fig. 12). The strong decrease of $\sigma^{\rm max}_{\gamma_{\rm SD}}$ in the $p4n$ channel in comparison with $4n$- and $5n$-evaporation channels is mainly determined by the smaller probability of proton emission from the DNS in comparison with that of neutron emission. In the reactions ^{82}Se(^{74}Ge, $4n$) and ^{80}Se(^{74}Ge, $2n$) $\sigma_{\rm cap}[^{82}$Se(^{74}Ge, $4n$)$]/\sigma_{\rm cap}[^{80}$Se(^{74}Ge, $2n$)$] \approx 2$ at optimal angular momentum $L^{\rm opt}_{\rm SD} \approx 50$ and,

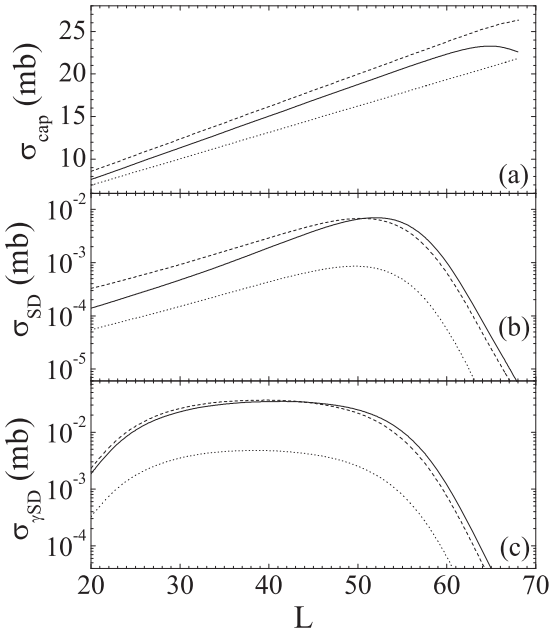

FIG. 12. The same as in Fig. 11, but for the reactions ^{120}Sn(^{36}S, 4n) (solid line), ^{124}Sn(^{33}S, 5n) (dashed line), and ^{120}Sn(^{37}Cl, $p4n$) (dotted line).

correspondingly, $\sigma_{SD}[^{82}\mathrm{Se}(^{74}\mathrm{Ge}, 4n)]/\sigma_{SD}[^{82}\mathrm{Se}(^{74}\mathrm{Ge}, 4n)] \approx \sigma^{max}_{\gamma_{SD}}[^{82}\mathrm{Se}(^{74}\mathrm{Ge}, 4n)]/\sigma^{max}_{\gamma_{SD}}[^{82}\mathrm{Se}(^{74}\mathrm{Ge}, 4n)] \approx 2$.

In all de-excitation channels considered, except for $\alpha 4n$, the ratio of the SD and ND band intensities in the maximum is about 0.01 (Figs. 10, 13, and 14). The optimal channel is the $4n$ channel (1.25%). For example, the maximal ratios are $I_{SD}/I_{ND} = 0.0108$, 0.009, and 0.008 in $2n$, $5n$, and $p4n$ channels, respectively. Note that in spite of $\sigma^{max}_{\gamma_{SD}}[^{120}\mathrm{Sn}(^{37}\mathrm{Cl}, p4n)] \ll \sigma^{max}_{\gamma_{SD}}[^{124}\mathrm{Sn}(^{33}S, 5n)]$, the maximal ratios $[I_{SD}/I_{ND}]_{^{120}\mathrm{Sn}(^{37}\mathrm{Cl}, p4n)} \approx [I_{SD}/I_{ND}]_{^{124}\mathrm{Sn}(^{33}\mathrm{S}, 5n)}$. We observe similar behavior in the reactions ^{82}Se(^{74}Ge, 4n) and ^{80}Se(^{74}Ge, 2n) (Fig. 13).

In the case of α emission, the evaporated α particle carries rather large orbital momentum $\Delta L = l_\alpha$ (Fig. 16), and the spin L of the populated SD state corresponds to the larger values of

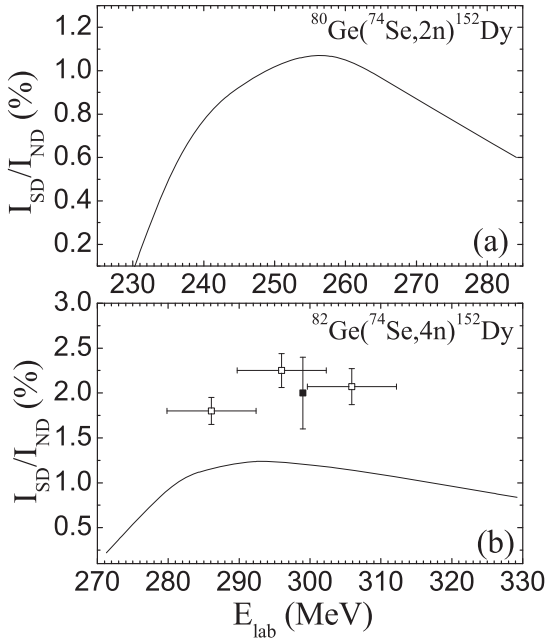

FIG. 13. The calculated ratio of the SD and ND band intensities (lines) in the ^{152}Dy nucleus as a function of beam energy in the reactions ^{80}Se(^{74}Ge, 2n) (a) and ^{82}Se(^{74}Ge, 4n) (b). The experimental data are from Refs. [10] (open squares) and [9] (closed squares).

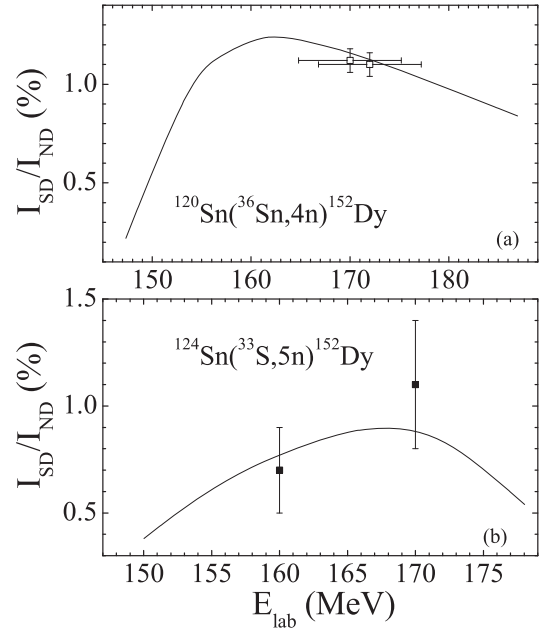

FIG. 14. The calculated ratio of the SD and ND band intensities (lines) in the ^{152}Dy nucleus as a function of beam energy in the reactions ^{120}Sn(^{36}S, 4n) (a) and ^{124}Sn(^{33}S, 5n) (b). The experimental data are from Refs. [10] (open squares) and [12] (closed squares).

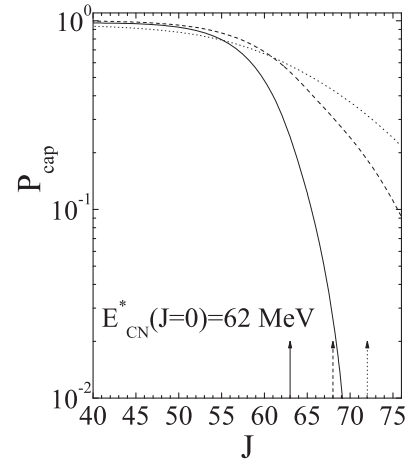

FIG. 15. The calculated capture probabilities in the reactions ^{120}Sn(^{36}S, 4n) (solid line), ^{108}Pd(^{48}Ca, 4n) (dashed line), and ^{82}Se(^{74}Ge, 4n) (dotted line) as functions of $L = J - \Delta L$ at the same excitation energy $E^*_{CN}(J = 0) = 62$ MeV of the CN. The maximal values of L, at which $E_{c.m.} = V_b(J)$ in these reactions, are denoted by arrows with the same lines as the capture probabilities.

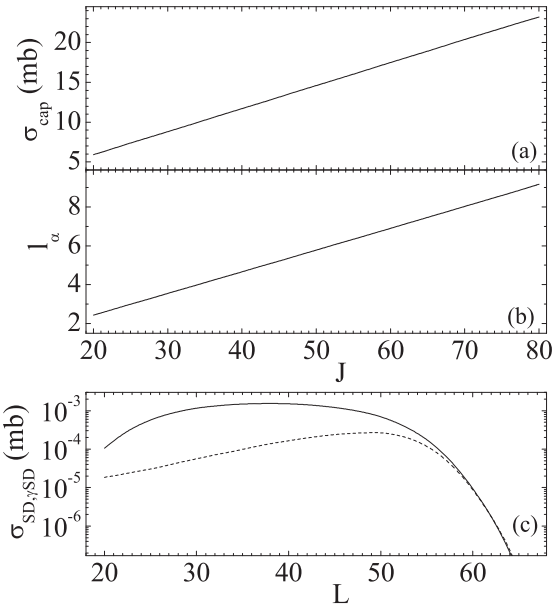

FIG. 16. The calculated dependencies of the capture cross section $\sigma_{\rm cap}(E_{\rm c.m.}, J)$ (a), the orbital momentum l_α carried out by emitted α particle on angular momentum J (b), and the cross sections $\sigma_{\rm SD}(E_{\rm c.m.}, L)$ and $\sigma_{\gamma_{\rm SD}}(E_{\rm c.m.}, L)$ as functions of spin L (c) in the ^{123}Sb(^{37}Cl, $\alpha 4n$) reaction at the optimal bombarding energy corresponding to the maximal ratio of the SD and ND band intensities.

initial angular momentum J than in xn- and pxn-evaporation channels. This leads to an increase of quasifission in the $\alpha 4n$ channel and a decrease of the value $I_{\rm SD}/I_{\rm ND}$ (Fig. 17). Here, the maximal ratio $I_{\rm SD}/I_{\rm ND}$ is 0.0039.

The optimal population (with the maximal $I_{\rm SD}/I_{\rm ND}$) of the SD band in ^{152}Dy occurs at a bombarding energy $E_{\rm c.m.} = E^{\rm opt}_{\rm c.m.}$

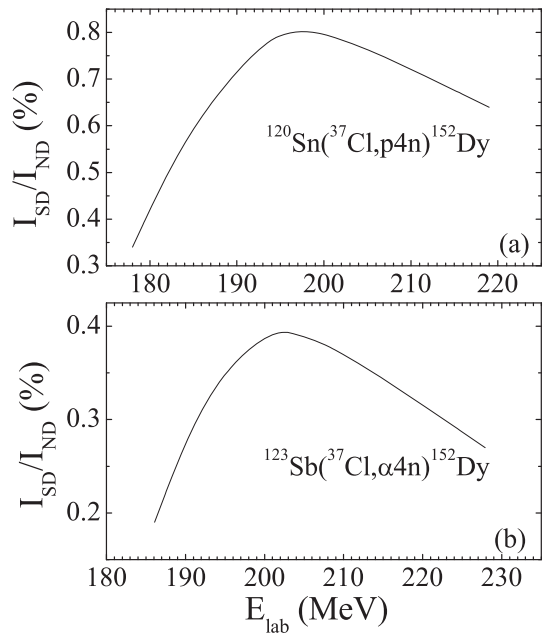

FIG. 17. The calculated ratio of the SD and ND band intensities in ^{152}Dy as a function of beam energy in the reactions ^{120}Sn(^{37}Cl, $p4n$) (a) and ^{123}Sb(^{37}Cl, $\alpha 4n$) (b).

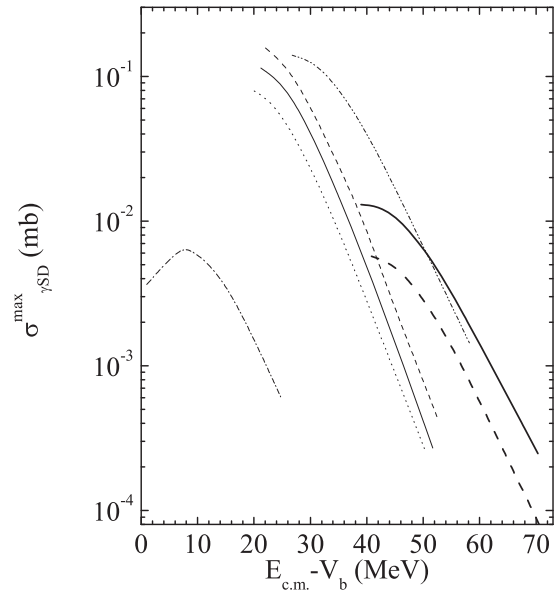

FIG. 18. The calculated dependencies of the cross sections $\sigma^{\rm max}_{\gamma_{\rm SD}}$ on $E_{\rm c.m.} - V_b(J = 0)$ for the reactions ^{108}Pd(^{48}Ca, $4n$) (solid line), ^{82}Se(^{74}Ge, $4n$) (dashed line), ^{80}Se(^{74}Ge, $2n$) (dash-dotted line), ^{120}Sn(^{36}S, $4n$) (dotted line), ^{124}Sn(^{33}S, $5n$) (dash-dot-dotted line), ^{120}Sn(^{37}Cl, $p4n$) (thick solid line), and ^{123}Sb(^{37}Cl, $\alpha 4n$) (thick dashed line). The intervals of the values of $E_{\rm c.m.}$ correspond to the beam energies in Figs. 13, 14, and 17. For the $4n$-, $5n$-, $p4n$-, and $\alpha 4n$-evaporations channels, only the right-hand sides of $\sigma^{\rm max}_{\gamma_{\rm SD}}$ are shown and the values of $\sigma^{\rm max}_{\gamma_{\rm SD}}$ at the lowest energies are close to the maxima.

much higher than the entrance Coulomb barrier $V_b = V_b(J = 0) = V(R_b, Z, A, \beta_1 = 0, \beta_2 = 0, J = 0)$ at $J = 0$ for all de-excitation channels, except for the $2n$ channel. Note that in all channels $E^{\rm opt}_{\rm c.m.} > V_b(J = L^{\rm opt}_{\rm SD})$, where the SD state with the optimal spin $L = L^{\rm opt}_{\rm SD}$ gives the largest contribution to $\sigma^{\rm max}_{\gamma_{\rm SD}}$. For example, in the ^{74}Ge + ^{80}Se reaction, $V_b(J = L^{\rm opt}_{\rm SD} \approx 50) = 133$ MeV and $E^{\rm opt}_{\rm c.m.} = 135$ MeV and at lower energies the values $\sigma^{\rm max}_{\gamma_{\rm SD}}$ and $I_{\rm SD}/I_{\rm ND}$ rapidly decrease (Figs. 13 and 18). From Fig. 18 one can conclude that the maxima of $\sigma^{\rm max}_{\gamma_{\rm SD}}$ are shifted by about 15 MeV to smaller energies with respect to the maxima of $I_{\rm SD}/I_{\rm ND}$ in the $4n$, $5n$, $p4n$, and $\alpha 4n$ channels. This means that with increasing $E_{\rm c.m.}$ the population of the ND states decreases faster than the population of the SD states. For the $2n$ channel, the energy positions of the maxima of $\sigma^{\rm max}_{\gamma_{\rm SD}}$ and $I_{\rm SD}/I_{\rm ND}$ are comparable.

IV. SUMMARY

Employing the DNS approach combined with dynamical and statistical methods, we studied the population of the yrast SD band in ^{152}Dy, produced in various de-excitation channels of the reactions with different entrance-channel asymmetries. It was shown that the spin population interval of the SD band is restricted from below by the complete fusion process and from above by the quasifission (DNS decay) process. For example, the $\alpha 4n$-evaporation channel is not the optimal one due to the arger initial angular momentum required because of the large orbital angular momentum carried by an α particle and, correspondingly, large suppression of the SD population

by quasifission. The excitation function for the population of the SD band shows the same trends as that for the complete fusion reactions but it has a much larger width. We found very weak dependencies of the SD transition intensities on the beam energy. No evidence for an entrance-channel effects is found in our model, in contradiction with the experimental data [9,10]. New experimental and theoretical studies of the entrance-channel effect are required.

The quite good agreement of our results with the experimental data indicates the validity of the DNS interpretation of strongly deformed nuclear states and supports predictions concerning the possible formation of highly deformed states in the entrance channel of heavy-ion reactions [43,44] (without the CN formation stage) based on the same theoretical approach. In future, it will be interesting to study the population of the SD bands of nuclei in the mass regions $A \approx 100$ and 190.

ACKNOWLEDGMENTS

This work was supported by RFBR under Grants No. 12-02-31355, No. 12-02-91159, No. 13-02-00080, and No. 13-02-12168. The IN2P3 (France)–JINR (Dubna) and Polish–JINR (Dubna) Cooperation Programmes are gratefully acknowledged.

APPENDIX A: CAPTURE PROBABILITY

The capture probability $P_{\rm cap}$ is obtained by integrating the propagator G from the initial phase space state (R_0, P_0) at time $t = 0$ to the final phase space state (R, P) at time t [51]:

$$P_{\rm cap} = \lim_{t\to\infty} \int_{-\infty}^{R_{\rm in}} dR \int_{-\infty}^{\infty} dP\, G(R, P, t|R_0, P_0, 0) = \lim_{t\to\infty} \frac{1}{2}{\rm erfc}\left[\frac{-R_{\rm in} + \overline{R(t)}}{\sqrt{\Sigma_{RR}(t)}}\right]. \quad \text{(A1)}$$

Here, P is the conjugate momentum. The second line in (A1) is obtained by using the propagator $G = \pi^{-1}|\det \Sigma^{-1}|^{1/2} \exp(-\mathbf{q}^T \Sigma^{-1} \boldsymbol{q})$ [with $q_R(t) = R - \overline{R(t)}$, $q_P(t) = P - \overline{P(t)}$, $\overline{R(t=0)} = R_0$, $\overline{P(t=0)} = P_0$, $\Sigma_{ij}(t) = 2\overline{q_i(t)q_j(t)}$, and $\Sigma_{ij}(t=0) = 0$, $i, j = R, P$] calculated in Ref. [52] for the inverted oscillator which approximates the nucleus-nucleus potential V in the variable R. The frequency ω of this oscillator with internal turning point $R_{\rm in}$ is defined from the condition of equality of the classical actions of approximated and realistic potential barriers of the same height at given J (Fig. 2). Many quantum-mechanical, dissipative, non-Markovian, neutron transfer, and deformation effects accompanying the passage through the potential barrier are taken into consideration in our formalism [53]. The derivation of equations for the first moment $\overline{R(t)}$ and variance $\Sigma_{RR}(t)$ in the coordinate is presented in Refs. [53,54].

APPENDIX B: PROBABILITY OF EMISSION OF A FIXED NUMBER OF NEUTRONS

In the case of the emission of x neutrons with binding energies B_{n_k} $(i = k, \ldots, x)$ from a system with initial excitation energy E, the probability to cool the system at the last xth evaporation step by neutron emission to an excitation energy smaller than $\delta = 0.2$ MeV, in order to consider it cold, is obtained by using the Maxwellian form of the neutron spectrum $\nu_n(\epsilon_n) = \epsilon_n \exp[-\epsilon_n/T]/T^2$:

$$w^x_{xn}(E_x) = \frac{\int_{E_x - B_{n_x} - \delta}^{E_x - B_{n_x}} \nu(\epsilon_n) d\epsilon_n}{\int_0^{E_x - B_{n_x}} \nu(\epsilon_n) d\epsilon_n}, \quad \text{(B1)}$$

where E_x is the excitation energy before the emission of the last neutron. Then the probability to cool the system by a sequence of neutron emission from the kth to xth evaporation steps is recursively defined as

$$w^k_{xn}(E_k) = \frac{\int_{\sum_{j=k+1}^{x} B_{n_j} + \delta}^{E_k - B_{n_k}} w^{k+1}_{xn}(E_{k+1}) \nu(E_k - B_{n_k} - E_{k+1}) dE_{k+1}}{\int_0^{E_k - B_{n_k}} \nu(E_k - B_{n_k} - E_{k+1}) dE_{k+1}}. \quad \text{(B2)}$$

Finally, $w^1_{xn}(E_1) \equiv w_{xn}(E)$.

APPENDIX C: INTERNAL EXCITATION ENERGIES OF QUASIFISSION FRAGMENTS

By using total energy conservation

$$E^{\rm total}_{\rm DNS}(J) = E^{\rm total}_{\rm QF}(l, J_1, J_2),$$

where

$$E^{\rm total}_{\rm DNS}(L) = B_1 + B_2 + V(R_m, Z, A, \beta_1, \beta_2, J = 0) + \frac{\hbar^2 J(J+1)}{2\Im} + E^*_{Z,A}(J)$$

is the total energy of the DNS with asymmetries (Z, A) and

$$E^{\rm total}_{\rm QF}(l, J_1, J_2) = B_1 + B_2 + TKE(l) + \frac{\hbar^2 J_1(J_1+1)}{2\Im_1} + \frac{\hbar^2 J_2(J_2+1)}{2\Im_2} + E^*_1(J_1) + E^*_2(J_2),$$
$$TKE(l) = V(R_b, Z, A, \beta_1, \beta_2, J = 0) + \frac{\hbar^2 l(l+1)}{2\mu R_b^2} + 2T_{Z,A}(J),$$

are the total energy and the total kinetic energy of the quasifission fragments, respectively, one can derive the sum of the internal excitation energies of quasifission fragments 1 and 2:

$$E^*_1 + E^*_2 = E^*_{Z,A}(J) - B^{qf}_R(Z, A, J = 0) - 2T_{Z,A}(J) + \frac{\hbar^2 J(J+1)}{2\Im} - \frac{\hbar^2 J_1(J_1+1)}{2\Im_1} - \frac{\hbar^2 J_2(J_2+1)}{2\Im_2} - \frac{\hbar^2 l(l+1)}{2\mu R_b^2}. \quad \text{(C1)}$$

Here, for simplicity, we assume that $k_0 = 1$. Since at the sticking limit $J_i = \frac{\Im_i}{\Im} J$ $(i = 1, 2)$ for the spins of fragments

and $l = \frac{\mu R_m^2}{\Im} J$ for the orbital angular momentum,

$$\frac{\hbar^2 J(J+1)}{2\Im} = \frac{\hbar^2 l(l+1)}{2\mu R_m^2} + \frac{\hbar^2 J_1(J_1+1)}{2\Im_1} + \frac{\hbar^2 J_2(J_2+1)}{2\Im_2},$$

and

$$B_{qf}(Z, A, J) = B_{qf}(Z, A, J=0) + \frac{\hbar^2 l(l+1)}{2\mu R_b^2} - \frac{\hbar^2 l(l+1)}{2\mu R_m^2},$$

then Eq. (B1) can be rewritten as

$$E_1^* + E_2^* = E_{Z,A}^*(J) - [B_{qf}(Z, A, J) + 2T_{Z,A}(J)]. \quad \text{(C2)}$$

By using Eq. (B2) and the relation $E_2^*/E_1^* = a_2/a_1$, where a_i are the level density parameters of fragment i, we obtain the internal excitation energies of the fragments as

$$E_{1,2}^* = \frac{a_{1,2}}{a_1 + a_2}\{(E_{Z,A}^*(J) - [B_{qf}(Z, A, J) + 2T_{Z,A}(J)]\}. \quad \text{(C3)}$$

If $a_i = A_i/b$, b is the constant; for example, if $b = 12\,\text{MeV}^{-1}$, the excitation energies of the fragments,

$$E_{1,2}^* = \frac{A_{1,2}}{A}\{E_{Z,A}^*(J) - [B_{qf}(Z, A, J) + 2T_{Z,A}(J)]\}, \quad \text{(C4)}$$

are proportional to their mass numbers. Assuming $a_1 = E_1^* = 0$ for the stiff magic α particle in the DNS, i.e., assuming that the α particle has no internal structure, we obtain the following simple formula for the internal excitation energy of the heavy quasifission fragment:

$$E_2^* = E_{Z,A}^*(J) - [B_{qf}(Z, A, J) + 2T_{Z,A}(J)]. \quad \text{(C5)}$$

[1] B. B. Buck, H. C. Britt, J. D. Garett, and O. Hansen, Phys. Rev. Lett. **28**, 1707 (1972).
[2] P. J. Twin, Nucl. Phys. A **520**, 17c (1990).
[3] P. J. Twin *et al.*, Phys. Rev. Lett. **57**, 811 (1986).
[4] M. A. Bentley *et al.*, Phys. Rev. Lett. **59**, 2141 (1987).
[5] T. Lauritsen *et al.*, Phys. Rev. Lett. **88**, 042501 (2002).
[6] T. Lauritsen *et al.*, Phys. Rev. C **75**, 064309 (2007).
[7] M. B. Smith *et al.*, Phys. Rev. C **61**, 034314 (2000).
[8] P. J. Twin, in *Proceedings of the Inter. Conference on Contemporary Topics in Nuclear Structure Physics, Cocoyoc, Mexico, 1988*, edited by R. F. Casten, A. Frank, M. Moshinsky, and S. Pittel (World Scientific, Singapore, 1988), p. 445.
[9] A. O. Macchiavelli, M. A. Deleplanque, R. M. Diamond, R. J. McDonald, F. S. Stephens, and J. E. Draper, Phys. Rev. C **36**, 2177 (1987).
[10] G. Smith *et al.*, Phys. Rev. Lett. **68**, 158 (1992).
[11] A. Nourreddine *et al.*, Phys. Rev. C **36**, 2687 (1987).
[12] L. Müller *et al.*, Z. Phys. A **341**, 131 (1992).
[13] D. C. Radford, A. Galindo-Uribarri, G. Hackman, and V. P. Janzen, Nucl. Phys. A **557**, 311 (1993).
[14] M. Aïche *et al.*, Eur. Phys. J A **6**, 121 (1999).
[15] S. Åberg, H. Flocard, and W. Nazarewicz, Annu. Rev. Nucl. Part. Sci. **40**, 439 (1990).
[16] M. Freer and A. C. Merchant, J. Phys. G **23**, 261 (1997).
[17] J. Cseh, A. Algora, J. Darai, and P. O. Hess, Phys. Rev. C **70**, 034311 (2004).
[18] J. Darai, J. Cseh, and D. G. Jenkins, Phys. Rev. C **86**, 064309 (2012).
[19] R. B. Wiringa, S. C. Pieper, J. Carlson, and V. R. Pandharipande, Phys. Rev. C **62**, 014001 (2000).
[20] Y. Kanada Enyo and H. Horiuchi, Prog. Theor. Phys. **142**, 205 (2001).
[21] W. Nörtershäuser, T. Neff, R. Sánchez, and I. Sick, Phys. Rev. C **84**, 024307 (2011).
[22] J. Cseh, G. Levai, A. Ventura, and L. Zuffi, Phys. Rev. C **58**, 2144 (1998).
[23] W. Sciani, Y. Otani, A. Lepine-Szily, E. A. Benjamim, L. C. Chamon, R. L. Filho, J. Darai, and J. Cseh, Phys. Rev. C **80**, 034319 (2009); J. Cseh, J. Darai, W. Sciani, Y. Otani, A. Lepine-Szily, E. A. Benjamim, L. C. Chamon, and R. L. Filho, *ibid.* **80**, 034320 (2009).
[24] N. Cindro, J. Phys. G **4**, L23 (1978); N. Cindro and W. Greiner, *ibid.* **9**, L175 (1983).
[25] W. Greiner, J. Y. Park, and W. Scheid, *Nuclear Molecules* (World Scientific, Singapore, 1995).
[26] S. J. Sanders, A. Szanto de Toledo, and C. Beck, Phys. Rep. **311**, 487 (1999).
[27] R. Nouicer *et al.*, Phys. Rev. C **60**, 041303(R) (1999).
[28] A. Morsad, F. Haas, C. Beck, and R. M. Freemann, Z. Phys. A **338**, 61 (1991); C. Beck *et al.*, Phys. Rev. C **63**, 014607 (2000).
[29] W. von Oertzen, V. Zherebchevsky, B. Gebauer, Ch. Schulz, S. Thummerer, D. Kamanin, G. Royer, and Th. Wilpert, Phys. Rev. C **78**, 044615 (2008); W. von Oertzen *et al.*, Eur. Phys. J. A **36**, 279 (2008).
[30] C. Beck *et al.*, Phys. Rev. C **80**, 034604 (2009).
[31] V. V. Pashkevich *et al.*, Nucl. Phys. A **624**, 140 (1997).
[32] T. Lauritsen *et al.*, Phys. Rev. Lett. **89**, 282501 (2002); T. L. Khoo *et al.*, *ibid.* **76**, 1583 (1996); G. Hackman *et al.*, *ibid.* **79**, 4100 (1997); A. Lopez-Martens *et al.*, Phys. Lett. B **380**, 18 (1996); J. R. Hughes *et al.*, Phys. Rev. C **50**, R1265 (1994); K. Hauschild *et al.*, *ibid.* **55**, 2819 (1997); A. N. Wilson *et al.*, *ibid.* **54**, 559 (1996); B. Crowell *et al.*, *ibid.* **51**, R1599 (1995); D. Rossbach *et al.*, *ibid.* **66**, 024316 (2002); Phys. Lett. B **513**, 9 (2001); U. J. van Severen *et al.*, Z. Phys. A **353**, 15 (1995); S. Bouneau *et al.*, *ibid.* **358**, 179 (1997); P. Fallon *et al.*, Phys. Rev. Lett. **73**, 782 (1994); A. Korichi *et al.*, *ibid.* **86**, 2746 (2001); A. Prevost *et al.*, Eur. Phys. J. A **10**, 13 (2001).
[33] S. Åberg, Nucl. Phys. A **557**, 17 (1993); Z. Phys. A **349**, 205 (1994).
[34] G. G. Adamian, N. V. Antonenko, R. V. Jolos, S. P. Ivanova, and A. K. Nasirov, in *Proceedings of the International Conference on Nuclear Structure and Nuclear Reactions at Low and Intermediate Energies* (Joint Institute for Nuclear Research, Dubna, 1993), p. 217.
[35] S. Cwiok, W. Nazarewicz, J. X. Saladin, W. Plociennik, and A. Johnson, Phys. Lett. B **322**, 304 (1994).
[36] G. Royer and F. Haddad, J. Phys. G **21**, 339 (1995).
[37] G. G. Adamian, N. V. Antonenko, R. V. Jolos, S. P. Ivanova, and O. I. Melnikova, Int. J. Mod. Phys. E **5**, 191 (1996).
[38] B. Buck, A. C. Merchant, and S. M. Perez, Phys. Rev. C **61**, 014310 (1999).

[39] T. M. Shneidman, G. G. Adamian, N. V. Antonenko, S. P. Ivanova, and W. Scheid, Nucl. Phys. A **671**, 119 (2000).
[40] G. G. Adamian, N. V. Antonenko, N. Nenoff, and W. Scheid, Phys. Rev. C **64**, 014306 (2001); in *Proceedings of the Symposium on Cluster Aspects of Quantum Many-Body Systems*, edited by K. Kato *et al*. (World Scientific, Singapore, 2002), p. 215; G. G. Adamian, A. V. Andreev, N. V. Antonenko, N. Nenoff, W. Scheid, and T. M. Shneidman, Heavy Ion Phys. **19**, 87 (2003); Acta Phys. Pol. B **34**, 2147 (2003); G. G. Adamian, N. V. Antonenko, and W. Scheid, Fizika B **12**, 21 (2003); S. N. Kuklin, G. G. Adamian, N. V. Antonenko, and W. Scheid, Int. J. Mod. Phys. E **17**, 2019 (2008).
[41] G. G. Adamian, N. V. Antonenko, R. V. Jolos, Yu. V. Palchikov, and W. Scheid, Phys. Rev. C **67**, 054303 (2003).
[42] G. G. Adamian, N. V. Antonenko, R. V. Jolos, Yu. V. Palchikov, W. Scheid, and T. M. Shneidman, Nucl. Phys. A **734**, 433 (2003); Phys. Rev. C **69**, 054310 (2004).
[43] A. S. Zubov, V. V. Sargsyan, G. G. Adamian, N. V. Antonenko, and W. Scheid, Phys. Rev. C **81**, 024607 (2010).
[44] A. S. Zubov, V. V. Sargsyan, G. G. Adamian, N. V. Antonenko, and W. Scheid, Phys. Rev. C **82**, 034610 (2010).
[45] K. Schiffer and B. Herskind, Nucl. Phys. A **520**, 521c (1990).
[46] G. G. Adamian, N. V. Antonenko, and W. Scheid, Nucl. Phys. A **678**, 24 (2000).
[47] S. Raman, C. W. Nestor, Jr., and P. Tikkanen, At. Data Nucl. Data Tables **78**, 1 (2001).
[48] G. Audi, A. M. Wapstra, and C. Thibault, Nucl. Phys. A **729**, 337 (2003).
[49] P. Möller *et al*., At. Data Nucl. Data Tables **59**, 185 (1995).
[50] G. G. Adamian, N. V. Antonenko, and W. Scheid, Phys. Rev. C **68**, 034601 (2003).
[51] V. V. Sargsyan, G. G. Adamian, N. V. Antonenko, and W. Scheid, Eur. Phys. J. A **45**, 125 (2010).
[52] V. V. Dodonov and V. I. Man'ko, in *Density Matrices and Wigner Functions of Quasiclassical Quantum Systems*, edited by A. A. Komar (Nova Science, Commack, 1987), Proc. Lebedev Phys. Inst. of Sciences, Vol. 167.
[53] V. V. Sargsyan, Z. Kanokov, G. G. Adamian, N. V. Antonenko, and W. Scheid, Phys. Rev. C **80**, 034606 (2009); **80**, 047603 (2009).
[54] G. G. Adamian, N. V. Antonenko, Z. Kanokov, and V. V. Sargsyan, Teor. Mat. Fiz. **145**, 87 (2005) [Theor. Math. Phys. **145**, 1443 (2006)]; Z. Kanokov, Yu. V. Palchikov, G. G. Adamian, N. V. Antonenko, and W. Scheid, Phys. Rev. E **71**, 016121 (2005); Yu. V. Palchikov, Z. Kanokov, G. G. Adamian, N. V. Antonenko, and W. Scheid, *ibid*. **71**, 016122 (2005).
[55] Sh. A. Kalandarov, G. G. Adamian, N. V. Antonenko, and W. Scheid, Phys. Rev. C **82**, 044603 (2010); **83**, 054611 (2011); Sh. A. Kalandarov, G. G. Adamian, N. V. Antonenko, W. Scheid, and J. P. Wieleczko, *ibid*. **84**, 064601 (2011).
[56] T. M. Shneidman, G. G. Adamian, N. V. Antonenko, and R. V. Jolos, Phys. Rev. C **74**, 034316 (2006).